

## NUMERICAL SIMULATION OF ELASTIC/ELECTROMAGNETIC WAVES PROPAGATION: URSIN'S APPROACH

David da Costa de Pinho <sup>1</sup>, Viatcheslav Ivanovich Priimenko <sup>2,3</sup>,  
Marcia Miranda Azeredo <sup>2</sup>

**ABSTRACT.** This work aims to present and implement a mathematical algorithm based on Ursin's formalism to numerically simulate the propagation of elastic and electromagnetic waves in stratified 3D media. One of the significant advantages of the Ursin formalism is that, under certain conditions, this method allows one to consider partial differential equations describing various dynamic physical processes in a single form. Unlike the original work of Ursin, in the case of Maxwell's equations, to describe the process of propagation of electromagnetic waves in air, we used a hyperbolic version of Maxwell's equations; and in the Earth's subsurface, a diffusion (parabolic) version. An analysis of the elastic/electromagnetic responses is carried out in this paper, proving the effectiveness of the mathematical algorithm through numerical simulations.

**Keywords:** stratified 3D media; elastic/electromagnetic waves; Ursin's method; numerical simulation.

**RESUMO.** O objetivo deste trabalho é apresentar e implementar numericamente um algoritmo matemático, baseado no formalismo de Ursin, para a simulação da propagação de ondas elásticas e eletromagnéticas em meios 3D estratificados. Uma das grandes vantagens do formalismo de Ursin é que este método permite, sob certas condições, tratar as equações diferenciais parciais que descrevem vários processos físicos dinâmicos diferentes em uma única forma. Diferente do trabalho original de Ursin, no caso das equações de Maxwell, para caracterizar o processo de propagação das ondas eletromagnéticas no ar, usamos uma versão hiperbólica das equações de Maxwell, e na subsuperfície da terra - uma versão de difusão (parabólica). Uma análise das respostas elásticas/eletromagnéticas é realizada neste artigo, comprovando a eficácia do algoritmo matemático através de simulações numéricas.

**Palavras-chave:** meio 3D estratificado; ondas elásticas/eletromagnéticas; método de Ursin; simulação numérica.

Corresponding author: David da Costa de Pinho

<sup>1</sup>Instituto Federal Fluminense - Campus Macaé, RJ, Brazil – E-mail: david.pinho@ifff.edu.br

<sup>2</sup>Universidade Estadual do Norte Fluminense Darcy Ribeiro - Campos Macaé, RJ, Brazil - E-mails: slava@lenep.uenf.br; marcia578@gmail.com

<sup>3</sup>Instituto Nacional de Ciência e Tecnologia - Geofísica de Petróleo (INCT-GP/CNPq/MEC), Brazil

## INTRODUCTION

Many types of research are being performed to carry out computational and numerical simulations that describe several physical phenomena related to oil prospecting or other minerals and physical phenomena related to earthquakes or other applications.

There are many works dedicated to developing and applying analytical and matrix methods for waves propagation analysis in stratified media composed of homogeneous layers; see, for instance, Thomson (1950); Haskell (1953); Brekhovskii (1960); Kuznetz and D'Erceville (1962); Molotkov (1984); Tygel and Hubral (1987); Mackay and Lakhtakia (2020). One of the forms of the matrix method, which was introduced by Ursin (1983) for the analysis of elastic and electromagnetic waves propagation, is now widely used in the study of physical processes in the stratified media. For example, the case of viscoelastic media was analyzed in Ursin and Stovas (2002), and for propagation in poroelastic media in low and high frequencies, see Azeredo and Priimenko (2015); Miranda and Priimenko (2017); Oliveira *et al.* (2018). White and Zhou (2006) showed how the electrokinetic system of equations, which models the electroseismic effect, can be written in a convenient mathematical form suggested by Ursin.

The organization of this article is as follows: In Section Statement of the Problems, from Lamé parameters plugged in Hooke's law, Cauchy's equations of motion and Maxwell's equations, we built two systems of partial differential equations (PDE's) that model the elastic and electromagnetic waves propagation in the 3D space. When the functions depend only on the depth, Fourier transforms are useful to turn the PDE's systems that model wave propagation into ordinary differential equations (ODE's) systems. This approach permits us to put the Lamé and Maxwell system in the Ursin format, which is very useful for analyzing wave processes in stratified media. It is necessary to say that unlike the original work of Ursin, in the case of Maxwell's equations, to describe the process of propagation of electromagnetic waves in air, we used the complete (hyperbolic) version of Maxwell's equations; and in the Earth's subsurface, a diffusion version. The resulting system of differential equations was considered when an external source of electromagnetic oscillations was located only in the subsurface. In addition, following Pride and Haarsten (1996); Haarsten and Pride (1997), the problem was reduced to a problem considered only in the earth's subsurface. In Section Ursin Method we shortly present the Ursin method, i.e., the Ursin diagonalization process, the reflection and transmission matrices, source and boundary conditions, representation of different types of sources. The derivation of the main formulas of the Ursin diagonalization process was organized somewhat differently. In Section Solution in Real Space we present the formulas, which permit calculating the obtained solution in the real space. Section Numeric Examples deals with the results of several nu-

merical experiments. They were implemented to illustrate the theoretical results in the previous sections. We built efficient computer codes that allow simulations of the elastic and electromagnetic waves propagating in a 3D stratified half-space. In Section Conclusion, we collected some additional comments. Finally, in the Appendix, we present the explicit formulas for the calculation of the eigenvalues and eigenvectors mentioned in Section Solution in Real Space for the considered elastic and electromagnetic problems.

## STATEMENT OF THE PROBLEMS

### Elastic Problem

We shall consider wave propagation in an isotropic elastic medium  $\mathcal{R}^+ = \cup_{n=0}^N \mathcal{R}_n$ , composed by stratified layers identified with  $\mathcal{R}_n = \{\mathbf{x} = (x, y, z) \in \mathbb{R}^3 : z_n < z < z_{n+1}\}$ , with  $0 = z_0 < z_1 \cdots < z_{N+1} = \infty$ . We assume that all material parameters are represented by piecewise constant functions depending only on the depth coordinate  $z$ , with the discontinuities at the points  $z = z_n, n = 1, 2, \dots, N$ .

In the temporal frequency ( $\omega$ ) domain (time dependence of  $e^{-i\omega t}$  is assumed), the Lamé equations are, at each point  $\mathbf{x} \in \mathbb{R}^3$ ,

$$\begin{aligned} -i\omega\rho\dot{\mathbf{u}} &= \nabla \cdot \boldsymbol{\tau} + \mathbf{f}, \\ -i\omega\boldsymbol{\tau} &= \lambda(\nabla \cdot \dot{\mathbf{u}})\mathbf{I} + G(\nabla\dot{\mathbf{u}} + \nabla\dot{\mathbf{u}}^T), \end{aligned} \quad (1)$$

see, for instance, Sokolnikoff (1946). Here  $\mathbf{f} = (f_1, f_2, f_3)^T$  is a vector-function characterizing an external elastic source;  $\dot{\mathbf{u}} = -i\omega\mathbf{u}$  is the solid velocity where  $\mathbf{u} = (u_1, u_2, u_3)^T$  is the displacement vector, and  $\boldsymbol{\tau}$  is the elastic stress tensor;  $\mathbf{I}$  is the  $3 \times 3$  identity matrix and  $^T$  means the transposition. The material parameters are as follows:  $\lambda$  and  $G$ , the Lamé coefficients;  $\rho$ , the material density.

For material parameters that depend only on the depth coordinate  $z$ , we take Fourier transforms in the two lateral coordinates  $x, y$ . Let  $(k_x, k_y)^T$  be the horizontal wavenumber and let

$$k = \sqrt{k_x^2 + k_y^2}, \quad \gamma = \frac{k}{\omega}$$

be the magnitude of the horizontal wavenumber and the horizontal slowness, respectively. Define the lateral Fourier transforms

$$\begin{aligned} \hat{\mathbf{f}}(k_x, k_y, z) &\equiv F(\mathbf{f}) \\ &= \iint_{\mathbb{R}^2} \mathbf{f}(x, y, z) e^{-i(k_x x + k_y y)} dx dy \end{aligned} \quad (2)$$

and

$$\begin{aligned} \mathbf{f}(x, y, z) &\equiv F^{-1}(\hat{\mathbf{f}}) \\ &= \frac{1}{4\pi^2} \iint_{\mathbb{R}^2} \hat{\mathbf{f}}(k_x, k_y, z) e^{i(k_x x + k_y y)} dk_x dk_y \end{aligned} \quad (3)$$

with similar expressions for the other variables.

**Note 1** The lateral Fourier transforms (2) and (3) have a different dependency from that adopted in the temporal transform (47).

Let us apply the lateral Fourier transform (2) to equations (1). The resulting system is greatly simplified if we rotate to a coordinate system  $\tilde{\mathbf{x}} = (\tilde{x}, \tilde{y}, \tilde{z})^T$  with the first coordinate oriented in the direction of the horizontal wavenumber  $(k_x, k_y)^T$ . By doing so, all plane waves have a spatial dependence of the form  $e^{ik\tilde{x}}$ . Therefore, the rotation matrix is

$$\Omega = \begin{pmatrix} \frac{k_x}{k} & \frac{k_y}{k} & 0 \\ -\frac{k_y}{k} & \frac{k_x}{k} & 0 \\ 0 & 0 & 1 \end{pmatrix}.$$

Define

$$\tilde{\mathbf{x}} = \Omega\hat{\mathbf{x}}, \quad \tilde{\mathbf{u}} = \Omega\hat{\mathbf{u}}, \quad \tilde{\boldsymbol{\tau}} = \Omega\hat{\boldsymbol{\tau}}\Omega^T, \quad \tilde{\mathbf{f}} = \Omega\hat{\mathbf{f}}. \quad (4)$$

Let

$$\Phi^{(1)} = [\dot{u}_3, \tilde{\tau}_{13}, \tilde{\tau}_{33}, \dot{u}_1]^T, \quad \Phi^{(2)} = [\dot{u}_2, \tilde{\tau}_{23}]^T, \quad (5)$$

and  $n_1 = 2$  and  $n_2 = 1$ . Then the  $2n_m$ -dimensional vectors  $\Phi^{(m)}$  satisfy uncoupled systems of linear ODE's of the Ursin form

$$\frac{d\Phi^{(m)}}{dz} = -i\omega\mathbf{M}^{(m)}\Phi^{(m)} + \mathbf{S}^{(m)}, \quad m = 1, 2, \quad (6)$$

where  $\mathbf{S}^{(m)}$  are  $2n_m$ -dimensional source vectors and the  $2n_m \times 2n_m$  matrices  $\mathbf{M}^{(m)}$  are of the block form

$$\mathbf{M}^{(m)} = \begin{pmatrix} \mathbf{0} & \mathbf{M}_1^{(m)} \\ \mathbf{M}_2^{(m)} & \mathbf{0} \end{pmatrix} \quad (7)$$

with symmetric  $n_m \times n_m$  submatrices

$$\mathbf{M}_1^{(m)} = \mathbf{M}_1^{(m)T}, \quad \mathbf{M}_2^{(m)} = \mathbf{M}_2^{(m)T}.$$

System 1 ( $m = 1$ ) contains compressional ( $P$ ) and vertical shear ( $SV$ ) waves. For this system we have

$$\mathbf{M}_1^{(1)} = \begin{pmatrix} \frac{1}{\lambda+2G} & \frac{\lambda\gamma}{\lambda+2G} \\ \frac{\lambda\gamma}{\lambda+2G} & \rho - \frac{4\gamma^2 G(\lambda+G)}{\lambda+2G} \end{pmatrix}, \quad (8)$$

$$\mathbf{M}_2^{(1)} = \begin{pmatrix} \rho & \gamma \\ \gamma & G^{-1} \end{pmatrix}, \quad \mathbf{S}^{(1)} = (0, -\tilde{f}_1, \tilde{f}_3, 0)^T.$$

Once  $\Phi^{(1)}$  has been determined, we may also compute two variables which are dependent only on System 1:

$$\tilde{\tau}_{11} = \gamma \frac{\lambda^2 - (\lambda + 2G)^2}{\lambda + 2G} \dot{u}_1 + \frac{\lambda}{\lambda + 2G} \tilde{\tau}_{33},$$

$$\tilde{\tau}_{22} = \gamma \frac{\lambda^2 - \lambda(\lambda + 2G)}{\lambda + 2G} \dot{u}_1 + \frac{\lambda}{\lambda + 2G} \tilde{\tau}_{33}.$$

System 2 ( $m = 2$ ) contains shear horizontal (SH)

waves. For this system, we obtain

$$\mathbf{M}_1^{(2)} = G^{-1},$$

$$\mathbf{M}_2^{(2)} = \rho - G\gamma^2, \quad \mathbf{S}^{(2)} = (0, -\tilde{f}_2)^T. \quad (9)$$

Once  $\Phi^{(2)}$  has been determined, we may also compute the variable which is dependent only on System 2:

$$\tilde{\tau}_{12} = -G\gamma\dot{u}_2.$$

At the internal layer boundaries  $z = z_n$ ,  $n = 1, 2, \dots, N$ , we use the continuity of  $\mathbf{u}$ , the normal components of  $\boldsymbol{\tau}$ ; see, for instance, Carcione (2007). It immediately applies

$$z = z_n : [\dot{\mathbf{u}}] = \mathbf{0}, \quad [\tilde{\tau}_{13}] = [\tilde{\tau}_{23}] = [\tilde{\tau}_{33}] = 0,$$

where  $[\cdot]$  is the jump of corresponding function across the discontinuity  $z = z_n$ .

The boundary conditions at the free surface  $z = 0$  are

$$z = 0 : \tilde{\tau}_{13} = \tilde{\tau}_{23} = \tilde{\tau}_{33} = 0.$$

And finally, at the infinity the solution satisfy the following radiation conditions:

$$\lim_{z \rightarrow \infty} \dot{\mathbf{u}} = \mathbf{0}.$$

## Electromagnetic Problem

We shall consider wave propagation in an isotropic electromagnetic medium  $\mathcal{R} = \mathcal{R}^- \cup \mathcal{R}^+$ , where  $\mathcal{R}^- = \{\mathbf{x} \in \mathbb{R}^3 : -\infty < z < z_0\}$  characterizes the air infinite layer. We assume that all material parameters are represented by piecewise constant functions depending only on the depth coordinate  $z$ , with the discontinuities at the points  $z = z_n$ ,  $n = 1, 2, \dots, N$ .

In the temporal frequency domain, the Maxwell equations are, at each point  $\mathbf{x} \in \mathbb{R}^3$ ,

$$\begin{aligned} \nabla \times \mathbf{E} &= i\omega\mu_0\mathbf{H} \\ \nabla \times \mathbf{H} &= \bar{\sigma}\mathbf{E} + \mathbf{j} \\ \nabla \cdot \mathbf{H} &= 0. \end{aligned} \quad (10)$$

Here  $\mathbf{E} = (E_1, E_2, E_3)^T$  is the electric field;  $\mathbf{H} = (H_1, H_2, H_3)^T$  is the magnetic field;  $\mathbf{j} = (j_1, j_2, j_3)^T$  is the external electromagnetic source; and  $\bar{\sigma} = \sigma - i\omega\epsilon$ . The material parameters of this system are as follows:  $\mu_0$ , the constant magnetic permeability;  $\epsilon$ , the electric permittivity;  $\sigma$ , the conductivity.

**Note 2** It is customary in the analysis of the Earth's interior to assume the quasi-static behavior of Maxwell's equations; see for instance Griffiths (1999). This means that  $\epsilon = \epsilon_0, \sigma = 0 \implies \bar{\sigma} = -i\omega\epsilon_0$  in the air, and in the Earth's interior we neglect by the displacement current  $-i\omega\epsilon\mathbf{E}$  formally assuming  $\epsilon = 0 \implies \bar{\sigma} = \sigma$ .

Applying only the lateral Fourier transform (2), we can directly represent the Maxwell equations (10) in the

Ursin form (6), avoiding the rotation  $\Omega$ , where

$$\Phi^{(1)} = [\hat{H}_2, \hat{E}_1]^T, \quad \Phi^{(2)} = [\hat{E}_2, -\hat{H}_1]^T, \quad (11)$$

and

$$\begin{aligned} \mathbf{M}_1^{(1)} &= \frac{\bar{\sigma}}{i\omega}, & \mathbf{M}_2^{(1)} &= -\mu_0 - i\frac{\omega\gamma^2}{\bar{\sigma}}, \\ \mathbf{S}^{(1)} &= \left(-\hat{j}_1, -\frac{i\gamma\omega}{\bar{\sigma}}\hat{j}_3\right)^T \end{aligned} \quad (12)$$

for System 1, and

$$\begin{aligned} \mathbf{M}_1^{(2)} &= -\mu_0, & \mathbf{M}_2^{(2)} &= \frac{\bar{\sigma}}{i\omega} + \frac{\gamma^2}{\mu_0}, \\ \mathbf{S}^{(2)} &= \left(0, -\hat{j}_2\right)^T \end{aligned} \quad (13)$$

for System 2.

Once  $\Phi^{(m)}$ ,  $m = 1, 2$ , have been determined, we may also compute the following variables:

$$\begin{aligned} \text{System 1 : } \hat{E}_3 &= -\frac{ik}{\bar{\sigma}}\hat{H}_2 - \frac{1}{\bar{\sigma}}\hat{j}_3, \\ \text{System 2 : } \hat{H}_3 &= \frac{\gamma}{\mu_0}\hat{E}_2. \end{aligned}$$

At the internal layer boundaries  $z = z_n$ ,  $n = 1, 2, \dots, N$ , we use the continuity of the tangential components of  $\mathbf{E}$  and  $\mathbf{H}$ . It immediately applies

$$z = z_n : [\hat{E}_k] = [\hat{H}_k] = 0, \quad k = 1, 2.$$

Following [Pride and Haarsten \(1996\)](#); [Haarsten and Pride \(1997\)](#), we can reduce the domain  $\mathcal{R}$  of study to the Earth's interior only, excluding the upper (air) infinite layer, i.e., to consider Eqs.(6), (11)–(13) in  $\mathcal{R}^+$  domain only with the following boundary conditions at the earth/air surface  $z = 0$

$$\begin{aligned} \text{System 1 : } \hat{H}_2 &= -\frac{\epsilon_0}{q_0}\hat{E}_1, \\ \text{System 2 : } \hat{H}_1 &= \frac{q_0}{\mu_0}\hat{E}_2, \end{aligned} \quad (14)$$

where  $q_0$  is the vertical slowness of an electromagnetic wave in the air, i.e.,

$$q_0 = \sqrt{\epsilon_0\mu_0 - \gamma^2}. \quad (15)$$

And finally, at the infinity, the solution satisfy the following radiation conditions:

$$\lim_{z \rightarrow \infty} \hat{E}_k = \lim_{z \rightarrow \infty} \hat{H}_k = 0, \quad k = 1, 2.$$

**Note 3** Note that this problem can also be solved using the same approach (with the rotation  $\Omega$ ) that was used to solve the problem of the propagation of elastic waves in a piecewise constant elastic medium.

### URSIN METHOD

As we have shown, we've been able to write the Lamé and Maxwell equations in a single form (6), which can be solved using the method proposed by [Ursin \(1983\)](#), divided into several steps described in the next section.

### Ursin diagonalization

We shortly present Ursin's diagonalization procedure in the form that it will be used here; see, for instance, [Azaredo and Priimenko \(2015\)](#) for detail. We consider matrices of the form (7) dropping the superscript  $(m)$  for simplicity.

Assume that  $\mathbf{M}_1\mathbf{M}_2$  has  $n$  distinct nonzero eigenvalues  $\lambda_j^2$ ,  $j = 1, 2, \dots, n$ , with associated eigenvectors  $\mathbf{a}_j$ , such that  $\mathbf{a}_j^T\mathbf{M}_2\mathbf{a}_j = \lambda_j$ . Here  $\lambda_j = \sqrt{\lambda_j^2}$  with the branch chosen so that  $\text{Im}(\lambda_j) \geq 0$  and  $\lambda_j > 0$  if  $\lambda_j$  is real. Define  $\mathbf{b}_j = \lambda_j^{-1}\mathbf{M}_2\mathbf{a}_j$ . This vector is an eigenvector of  $\mathbf{M}_2\mathbf{M}_1$  with eigenvalue  $\lambda_j^2$ . Using the symmetries of  $\mathbf{M}_1$  and  $\mathbf{M}_2$ , we obtain  $\mathbf{a}_j^T\mathbf{b}_i = \delta_j^i$ , where  $\delta_j^i$  is the Kronecker delta.

Let  $\mathbf{L}_1$  be the  $n \times n$ -matrix whose  $j$ -th column is  $\mathbf{a}_j$ , and let  $\mathbf{L}_2$  be the  $n \times n$ -matrix whose  $i$ -th column is  $\mathbf{b}_i$ , then  $\mathbf{L}_1^{-1} = \mathbf{L}_2^T$ ,  $\mathbf{L}_2^{-1} = \mathbf{L}_1^T$ . Introduce  $\mathbf{\Lambda} = \text{diag}(\lambda_1, \lambda_2, \dots, \lambda_n)$ . Then  $\mathbf{L}_2\mathbf{\Lambda} = \mathbf{M}_2\mathbf{L}_1$  and  $\mathbf{M}_1\mathbf{L}_2 = \mathbf{L}_1\mathbf{\Lambda}$ , which implies

$$\mathbf{M}_1 = \mathbf{L}_1\mathbf{\Lambda}\mathbf{L}_1^T, \quad \mathbf{M}_2 = \mathbf{L}_2\mathbf{\Lambda}\mathbf{L}_2^T. \quad (16)$$

Introducing the diagonal matrix  $\tilde{\mathbf{\Lambda}} = \text{diag}(\mathbf{\Lambda}, -\mathbf{\Lambda})$  and using (16), we finally obtain

$$\mathbf{M} = \mathbf{L}\tilde{\mathbf{\Lambda}}\mathbf{L}^{-1}, \quad (17)$$

where

$$\mathbf{L} = \frac{1}{\sqrt{2}} \begin{pmatrix} \mathbf{L}_1 & \mathbf{L}_1 \\ \mathbf{L}_2 & -\mathbf{L}_2 \end{pmatrix}, \quad \mathbf{L}^{-1} = \frac{1}{\sqrt{2}} \begin{pmatrix} \mathbf{L}_2^T & \mathbf{L}_1^T \\ \mathbf{L}_2^T & -\mathbf{L}_1^T \end{pmatrix}.$$

### Reflection and transmission matrices

Firstly, we consider a homogeneous source-free region of space. Dropping  $(m)$  we have a  $2n$ -dimensional system of the form (6) with  $\mathbf{M}$  constant and  $\mathbf{S} = \mathbf{0}$ . Let

$$\Phi = \mathbf{L}\Psi \quad \text{and} \quad \Psi = (\mathbf{U}, \mathbf{D})^T, \quad (18)$$

where  $\mathbf{U}$  and  $\mathbf{D}$  are  $n$ -vectors. Inserting (18) into (6) and using (17) we arrive at

$$\frac{d}{dz}\Psi = -i\omega\tilde{\mathbf{\Lambda}}\Psi.$$

Then

$$\Psi(z) = (e^{-i\omega\mathbf{\Lambda}(z-z_0)}\mathbf{U}(z_0), e^{i\omega\mathbf{\Lambda}(z-z_0)}\mathbf{D}(z_0))^T, \quad (19)$$

where  $z_0$  is a fixed point in the same source-free region. The vectors  $\mathbf{U}$  and  $\mathbf{D}$  characterize up-going ( $\mathbf{U}$ ) and down-going ( $\mathbf{D}$ ) waves. Next, consider an interface

at  $z = \bar{z}$ , where the material parameters vary discontinuously across  $\bar{z}$ . We denote by  $\pm$  quantities evaluated at  $\bar{z}^\pm = \bar{z} \pm 0$ . Since  $\Phi$  is continuous across  $\bar{z}$ , we obtain

$$\Psi^+ = J\Psi^-, \quad \Psi^- = J^{-1}\Psi^+, \quad (20)$$

where the jump matrix is

$$\mathbf{J} = (\mathbf{L}^+)^{-1}\mathbf{L}^- = \begin{pmatrix} \mathbf{J}_A & \mathbf{J}_B \\ \mathbf{J}_B & \mathbf{J}_A \end{pmatrix},$$

$$\mathbf{J}^{-1} = \begin{pmatrix} \mathbf{J}_A^T & -\mathbf{J}_B^T \\ -\mathbf{J}_B^T & \mathbf{J}_A^T \end{pmatrix},$$

and  $\mathbf{J}_A, \mathbf{J}_B$  are the  $n \times n$  matrices

$$\mathbf{J}_A = \frac{1}{2}[(\mathbf{L}_2^+)^T\mathbf{L}_1^- + (\mathbf{L}_1^+)^T\mathbf{L}_2^-],$$

$$\mathbf{J}_B = \frac{1}{2}[(\mathbf{L}_2^+)^T\mathbf{L}_1^- - (\mathbf{L}_1^+)^T\mathbf{L}_2^-].$$

Next, we consider a stack of layers  $0 < z_1 < \dots < z_N < \infty$ . We denote by subscript  $j$  a quantity at interface  $z = z_j$ , with superscripts  $\pm$  as before. Then

$$(\mathbf{U}_N^-, \mathbf{D}_N^-)^T = \mathbf{J}_N^{-1}(\mathbf{0}, \mathbf{D}_N^+)^T,$$

where we have used that there is no up-going wave below the last interface at  $z = z_N$ . So, we obtain

$$\mathbf{U}_N^- = \mathbf{\Gamma}_N \mathbf{D}_N^-, \quad \mathbf{D}_N^+ = \mathbf{T}_N \mathbf{D}_N^-,$$

where

$$\mathbf{\Gamma}_N = -\mathbf{J}_{B,N}^T (\mathbf{J}_{A,N}^T)^{-1}, \quad \mathbf{T}_N = (\mathbf{J}_{A,N}^T)^{-1}. \quad (21)$$

Here  $\mathbf{\Gamma}_N$  is the reflection matrix and  $\mathbf{T}_N$  is the transmission matrix from the last interface  $z = z_N$ .

Let  $j < N$  and  $\Delta z_j = z_{j+1} - z_j$ ,  $j = 0, 1, \dots, N-1$ , be the layer thickness. Then by jumping across the layer boundary and using (19) and (20) we obtain

$$\mathbf{U}_j^- = \mathbf{J}_{A,j}^T e^{i\omega\Lambda_j\Delta z_j} \mathbf{U}_{j+1}^- - \mathbf{J}_{B,j}^T e^{-i\omega\Lambda_j\Delta z_j} \mathbf{D}_{j+1}^-$$

$$\mathbf{D}_j^- = -\mathbf{J}_{B,j}^T e^{i\omega\Lambda_j\Delta z_j} \mathbf{U}_{j+1}^- + \mathbf{J}_{A,j}^T e^{-i\omega\Lambda_j\Delta z_j} \mathbf{D}_{j+1}^-.$$
(22)

Define reflection and transmission matrices  $\mathbf{\Gamma}_j, \mathbf{T}_j$  by the relations for any incident wave  $\mathbf{D}_j^-$  at the top of the stack of layers underlying  $z = z_j$

$$\mathbf{U}_j^- = \mathbf{\Gamma}_j \mathbf{D}_j^-, \quad \mathbf{D}_j^+ = \mathbf{T}_j \mathbf{D}_j^-. \quad (23)$$

Therefore  $\mathbf{\Gamma}_j$  computes the reflected wave from the stack, and  $\mathbf{T}_j$  computes the transmitted wave below the stack when the incident wave is known. From (22), (23) we obtain by induction

$$\mathbf{\Gamma}_j = (\mathbf{J}_{A,j}^T \tilde{\mathbf{\Gamma}}_{j+1} - \mathbf{J}_{B,j}^T) (-\mathbf{J}_{B,j}^T \tilde{\mathbf{\Gamma}}_{j+1} + \mathbf{J}_{A,j}^T)^{-1}$$

$$\mathbf{T}_j = \mathbf{T}_{j+1} e^{i\omega\Lambda_j\Delta z_j} (-\mathbf{J}_{B,j}^T \tilde{\mathbf{\Gamma}}_{j+1} + \mathbf{J}_{A,j}^T)^{-1},$$
(24)

where  $\tilde{\mathbf{\Gamma}}_{j+1} = e^{i\omega\Lambda_j\Delta z_j} \mathbf{\Gamma}_{j+1} e^{i\omega\Lambda_j\Delta z_j}$ . Again, by induction it can be shown that  $\mathbf{\Gamma}_j$  is symmetric.

Thus, all the reflection and transmission matrices can be calculated by (24), starting with (21).

### Sources and boundary conditions

Consider again a  $2n$ -dimensional system of the form (6) with  $(m)$  omitted. Let the source be of the form

$$\mathbf{S} = \mathbf{S}_0 \delta(z - z_s) + \mathbf{S}_1 \delta'(z - z_s) \quad (25)$$

with  $\mathbf{S}_0$  and  $\mathbf{S}_1$  independent of  $z$ . Here  $\delta$  is the Dirac function.

Let

$$\Phi_0 = \Phi - \mathbf{S}_1 \delta(z - z_s). \quad (26)$$

Then from (25), (26), and (6),

$$\frac{d\Phi_0}{dz} = -i\omega \mathbf{M} \Phi_0 + [\mathbf{S}_0 - i\omega \mathbf{M} \mathbf{S}_1] \delta(z - z_s). \quad (27)$$

Define  $n$ -vectors  $\mathbf{S}_A$  and  $\mathbf{S}_B$  by the following formula

$$(\mathbf{S}_A, \mathbf{S}_B)^T = i\omega \mathbf{M} \mathbf{S}_1 - \mathbf{S}_0. \quad (28)$$

Integrating (27) over an interval  $(z_s - \epsilon, z_s + \epsilon)$  with  $\epsilon \rightarrow 0$ , we obtain the following jump condition across the source

$$\Phi(z_s^-) = \Phi(z_s^+) + (\mathbf{S}_A, \mathbf{S}_B)^T. \quad (29)$$

Inserting a fictitious layer boundary at  $z = z_s^+$ , we compute the reflection matrix  $\mathbf{\Gamma}_s \equiv \mathbf{\Gamma}(z_s^+)$  from the top of this layer. Note that at  $z_s^+$ ,  $\mathbf{J}_A = \mathbf{I}$  and  $\mathbf{J}_B = \mathbf{0}$ , since the material properties do not change at  $z_s$ . Then the up-going wave  $\mathbf{U}_s \equiv \mathbf{U}_s(z_s^+)$  is related to the down-going wave  $\mathbf{D}_s \equiv \mathbf{D}_s(z_s^+)$  there by (23). Then we have

$$\Psi(z_s^+) = (\mathbf{\Gamma}_s \mathbf{D}_s, \mathbf{D}_s)^T. \quad (30)$$

Using (18), (29) and (30), we obtain

$$\Psi(z_s^-) = (\mathbf{\Gamma}_s \mathbf{D}_s, \mathbf{D}_s)^T$$

$$+ \frac{1}{\sqrt{2}} (\mathbf{L}_2^T \mathbf{S}_A + \mathbf{L}_1^T \mathbf{S}_B, \mathbf{L}_2^T \mathbf{S}_A - \mathbf{L}_1^T \mathbf{S}_B)^T.$$

This expression may now be propagated upwards through the layers, using (19) and jumped upwards across layers boundaries using (20) until we reach the free surface at  $z = 0^+$ . Then the  $n$  boundary conditions at  $z = 0$  can be used to find the  $n$  unknowns  $\mathbf{D}_s$ .

Consider now one particular case when  $z_s \in (0, z_1)$ . In this case

$$\Psi(0^+) = (e^{i\omega\Lambda_s z_s} \mathbf{\Gamma}_s \mathbf{D}_s, e^{-i\omega\Lambda_s z_s} \mathbf{D}_s)^T$$

$$+ \frac{1}{\sqrt{2}} (e^{i\omega\Lambda_s z_s} (\mathbf{L}_2^T \mathbf{S}_A + \mathbf{L}_1^T \mathbf{S}_B),$$

$$e^{-i\omega\Lambda_s z_s} (\mathbf{L}_2^T \mathbf{S}_A - \mathbf{L}_1^T \mathbf{S}_B))^T. \quad (31)$$

We next write

$$\Phi(0^+) = (\mathbf{G}_A \Phi_0, \mathbf{G}_B \Phi_0)^T, \quad (32)$$

where  $\Phi_0$  is an  $n$ -vector of unknowns at  $z = 0$  and  $\mathbf{G}_A, \mathbf{G}_B$  are  $n \times n$  matrices. Using (18), (31) and (32) we obtain

$$\begin{aligned} \Phi_0 &= \left( e^{i\omega\Lambda z_s} \Gamma_s e^{i\omega\Lambda z_s} (\mathbf{L}_2^T \mathbf{G}_A - \mathbf{L}_1^T \mathbf{G}_B) \right. \\ &\quad \left. - (\mathbf{L}_2^T \mathbf{G}_A + \mathbf{L}_1^T \mathbf{G}_B) \right)^{-1} e^{i\omega\Lambda z_s} \\ &\quad \times \left( \Gamma_s (\mathbf{L}_2^T \mathbf{S}_A - \mathbf{L}_1^T \mathbf{S}_B) - (\mathbf{L}_2^T \mathbf{S}_A + \mathbf{L}_1^T \mathbf{S}_B) \right), \\ \mathbf{D}_s &= \frac{1}{\sqrt{2}} e^{i\omega\Lambda z_s} (\mathbf{L}_2^T \mathbf{G}_A - \mathbf{L}_1^T \mathbf{G}_B) \Phi_0 \\ &\quad - \frac{1}{\sqrt{2}} (\mathbf{L}_2^T \mathbf{S}_A - \mathbf{L}_1^T \mathbf{S}_B). \end{aligned} \quad (33)$$

In particular, when the source is situated just below the surface, we get

$$\begin{aligned} \Phi_0 &= \left( (\Gamma_s - \mathbf{I}) \mathbf{L}_2^T \mathbf{G}_A - (\Gamma_s + \mathbf{I}) \mathbf{L}_1^T \mathbf{G}_B \right)^{-1} \\ &\quad \times \left( (\Gamma_s - \mathbf{I}) \mathbf{L}_2^T \mathbf{S}_A - (\Gamma_s + \mathbf{I}) \mathbf{L}_1^T \mathbf{S}_B \right) \end{aligned} \quad (34)$$

as  $z_s \rightarrow 0^+$ .  $\Phi_0$  defines all of  $\Phi$  at the free surface, and  $\mathbf{D}_s, \mathbf{U}_s = \Gamma_s \mathbf{D}_s$  give all of  $\Phi$  just below the source. Now we are able to compute  $\Phi$  in any  $z \in \mathbb{R}_+$  by propagating through the layers using (19) and (20).

**Note 4** Propagation of an upward-going wave in the downward direction will be unstable numerically using (19) because the complex exponentials grow rather than decay with distance. Therefore, numerically one has to obtain  $\mathbf{U}$  from  $\mathbf{D}$  using the reflection or transmission matrices.

**Types of sources**

In this section, we consider several examples of possible elastic and electromagnetic sources.

**Elastic case**

**Dynamite source.** A dynamite source can be defined in the following form

$$\mathbf{f}(x) = -s(\omega) \nabla \delta(x - x_s),$$

where  $x_s = (0, 0, z_s)^T$  is the source position and  $s(\omega)$  is the spectrum of the source moment  $s(t)$ . Applying the lateral Fourier transform (2) we obtain

$$\hat{\mathbf{f}} = -s(\omega) (ik_x \delta(z - z_s), ik_y \delta(z - z_s), \delta'(z - z_s))^T.$$

The rotation by  $\Omega$  yields

$$\tilde{\mathbf{f}} = -s(\omega) (ik \delta(z - z_s), 0, \delta'(z - z_s))^T. \quad (35)$$

Substitution of (35) into (8) gives the source for Sys-

tem 1 in the form (25) with

$$\mathbf{S}_0^{(1)} = ik_s(\omega) (0, 1, 0, 0)^T, \quad \mathbf{S}_1^{(1)} = s(\omega) (0, -1)^T. \quad (36)$$

Substitution of (35) into (9) shows that  $\mathbf{S}^{(2)}$  is zero, then  $\tilde{v}_2, \tilde{\tau}_{23}$  associated with System 2 are zero too. This is to be a expected result because System 2 is related to SH-waves, which are not excited by the dynamite source. Substitution of (36) into (28) gives

$$\mathbf{S}_A^{(1)} = i\omega(\lambda + 2G)s(\omega) (0, 1)^T, \quad \mathbf{S}_B^{(1)} = (0, 0)^T. \quad (37)$$

Formulas (37) may be used in (33) or (34) for a shallow source, to obtain all the tilde ( $\tilde{\phantom{x}}$ ) functions.

**Vertical source.** We next consider a vertical point source acting on the Earth's surface, i.e.,

$$\mathbf{f}(\mathbf{x}) = (0, 0, 1)^T s(\omega) \delta(x) \delta(y) \delta(z - z_s), \quad (38)$$

where  $z_s \rightarrow 0^+$  puts the source on the Earth's surface  $z = 0$ . This models hammer, weight drop, and vibroseis sources. Applying the lateral Fourier transform (6) and rotation  $\Omega$ , we arrive at

$$\tilde{\mathbf{f}} = \hat{\mathbf{f}} = (0, 0, 1)^T s(\omega) \delta(z - z_s). \quad (39)$$

Substitution of (39) into (8) and (9) yields the sources for Systems 1 and 2 in the form

$$\begin{aligned} \text{System 1 : } \mathbf{S}^{(1)} &= (0, 0, 1, 0)^T s(\omega) \delta(z - z_s), \\ \text{System 2 : } \mathbf{S}^{(2)} &= (0, 0)^T. \end{aligned}$$

In the case of System 1 we obtain the following expression from (25), (28) and (38):

$$\mathbf{S}_A^{(1)} = (0, 0)^T, \quad \mathbf{S}_B^{(1)} = s(\omega) (1, 0)^T.$$

In the case of System 2, all the variables are zero, as it was in the case of dynamite source.

**Electromagnetic case**

The Ursin form of the Maxwell equations was obtained without the application of rotation  $\Omega$ . For this reason, the electromagnetic source can be directly incorporated in the Ursin form of the electromagnetic equations.

**Source current in a plane.** We consider the distribution of source currents in the source plane  $z = z_s$ . Because of linearity and horizontal translation invariance, we need only to consider a point dipole at  $\mathbf{x} = (0, 0, z_s)^T$ , with source current

$$\mathbf{j} = \mathbf{j}^0 \delta(x) \delta(y) \delta(z - z_s), \quad \mathbf{j}^0 = (j_1^0, j_2^0, j_3^0)^T. \quad (40)$$

Solutions for other sources in the plane  $z = z_s$  can be synthesized by translation and superposition of sources of this type.

Applying to (40) the lateral Fourier transform (6), we arrive at

$$\mathbf{j} = \mathbf{j}^0 \delta(z - z_s). \quad (41)$$

Substitution of (41) into (12) and (13) yields the sources for electromagnetic Systems 1 and 2 in the form

$$\begin{aligned} \text{System 1 : } \mathbf{S}^{(1)} &= \left( -j_1^0, -\frac{i\gamma\omega}{\sigma} j_3^0 \right)^T, \\ \text{System 2 : } \mathbf{S}^{(2)} &= (0, -j_2^0)^T. \end{aligned}$$

In the case of System 1 we obtain the following expression from (25), (28) and (40):

$$\mathbf{S}_A^{(1)} = j_1^0 \quad \text{and} \quad \mathbf{S}_B^{(1)} = \frac{i\gamma\omega}{\sigma} j_3^0.$$

Similarly for System 2:

$$\mathbf{S}_A^{(2)} = 0 \quad \text{and} \quad \mathbf{S}_B^{(2)} = j_2^0.$$

### SOLUTION IN REAL SPACE

#### Elastic problem

From the tilde variables, the lateral Fourier transforms, i.e., the hat variables, can be computed by inverting the rotation in (4). Note that the matrices for Systems 1 and 2 depend only on the magnitude,  $k$  (or equivalently on the slowness  $\gamma$ ), of the vector  $(k_x, k_y)^T$  and not on its direction. However, factors of  $k_x$  and  $k_y$  are introduced by inverse rotation  $\Omega^{-1}$  and possibly by the directionality of the source. For any function  $\hat{h}(k)$  let

$$\begin{aligned} \mathcal{T}_{j_1, j_2}(\hat{h}) &\equiv F^{-1}(k_x^{j_1} k_y^{j_2} \hat{h}(k)) \\ &= (-i)^{j_1 + j_2} \left( \frac{\partial}{\partial x} \right)^{j_1} \left( \frac{\partial}{\partial y} \right)^{j_2} F^{-1}(\hat{h}(k)). \end{aligned} \quad (42)$$

We can compute these quantities as Hankel transforms in the cylindrical coordinates  $r, \theta, z$ ; see, for instance, [Bracewell \(1978\)](#). Define

$$B_{j_1, j_2}(\hat{h}) = \frac{1}{2\pi} \int_0^\infty k^{j_1} J_{j_2}(kr) \hat{h}(k) dk, \quad (43)$$

where  $J_{j_2}$  is the Bessel function and  $j_1, j_2$  are nonnegative integers. Then

$$\begin{aligned} \mathcal{T}_{0,0} &= B_{1,0}, \\ \mathcal{T}_{1,0} &= i \cos \theta B_{2,1}, \quad \mathcal{T}_{0,1} = i \sin \theta B_{2,1}, \\ \mathcal{T}_{1,1} &= \sin \theta \cos \theta \left( B_{3,0} - \frac{2}{r} B_{2,1} \right), \\ \mathcal{T}_{2,0} &= \cos^2 \theta B_{3,0} - \frac{\cos 2\theta}{r} B_{2,1}, \\ \mathcal{T}_{0,2} &= \sin^2 \theta B_{3,0} + \frac{\cos 2\theta}{r} B_{2,1}. \end{aligned} \quad (44)$$

To invert the rotation  $\Omega$ , note that from (5) and the vanishing of System 2,  $\hat{u}_2, \hat{\tau}_{12}, \hat{\tau}_{23}$  are identically zero. All the remaining tilde functions depend only on  $k$  and can

be calculated by the following formulas

$$\begin{aligned} \hat{u}_1 &= \frac{k_x}{k} \hat{u}_1, \quad \hat{u}_2 = \frac{k_y}{k} \hat{u}_1, \quad \hat{u}_3 = \hat{u}_3 \\ \hat{\tau}_{11} &= \frac{k_1^2 \tilde{\tau}_{11} + k_2^2 \tilde{\tau}_{22}}{k^2}, \quad \hat{\tau}_{12} = \frac{k_x k_y (\tilde{\tau}_{11} - \tilde{\tau}_{22})}{k^2} \\ \hat{\tau}_{22} &= \frac{k_2^2 \tilde{\tau}_{11} + k_1^2 \tilde{\tau}_{22}}{k^2}, \quad \hat{\tau}_{13} = \frac{k_x \tilde{\tau}_{13}}{k}, \\ \hat{\tau}_{13} &= \frac{k_y \tilde{\tau}_{13}}{k}, \quad \hat{\tau}_{33} = \tilde{\tau}_{33}. \end{aligned} \quad (45)$$

Formulas (45) can be inverted in cylindrical coordinates  $(r, \theta, z)$ , using (42)–(44), to real space:

$$\begin{aligned} \hat{\mathbf{u}} &= (iB_{1,1}(\hat{u}_1)) \mathbf{e}_r + (B_{1,0}(\hat{u}_3)) \mathbf{e}_z \\ \tau_{11} &= \mathcal{T}_{2,0}(k^{-2} \tilde{\tau}_{11}) + \mathcal{T}_{0,2}(k^{-2} \tilde{\tau}_{22}), \\ \tau_{12} &= \mathcal{T}_{1,1}(k^{-2} (\tilde{\tau}_{11} - \tilde{\tau}_{22})) \\ \tau_{22} &= \mathcal{T}_{0,2}(k^{-2} \tilde{\tau}_{11}) + \mathcal{T}_{2,0}(k^{-2} \tilde{\tau}_{22}), \\ \tau_{13} &= \mathcal{T}_{1,0}(k^{-1} \tilde{\tau}_{13}), \quad \tau_{23} = \mathcal{T}_{0,1}(k^{-1} \tilde{\tau}_{13}), \\ \tau_{33} &= \mathcal{T}_{0,0}(\tilde{\tau}_{33}). \end{aligned} \quad (46)$$

Here  $\mathbf{e}_r$  and  $\mathbf{e}_z$  are unit vectors in the  $r$  and  $z$  directions, respectively. Thus, the velocity  $\hat{\mathbf{u}}$  and the stress tensor  $\tau$  may be computed in cylindrical coordinates from (46) using transforms (43) and (44) of appropriate tilde functions. After that, all the variables can be computed in the time domain through the inverse Fourier transform

$$h(t) = \frac{1}{2\pi} \int_{\mathbb{R}} h(\omega) e^{-i\omega t} d\omega. \quad (47)$$

#### Electromagnetic problem

The solution to the electromagnetic problem was obtained without the application of the rotation  $\Omega$ . For this reason, the solution in real space will be the following

$$\mathbf{E} = B_{0,0}(\hat{\mathbf{E}}), \quad \mathbf{H} = B_{0,0}(\hat{\mathbf{H}}).$$

After that, all the variables can be computed in the time domain, applying the inverse Fourier transform (47).

### NUMERICAL EXAMPLES AND DISCUSSION

Table 1 shows the values of the parameters used in the numerical simulations.

For both elastic and electromagnetic waves, the blue color indicates the trace calculated using the real part of the obtained solutions; and red, their imaginary part.

#### Elastic waves simulation

Consider a particular case of the vertical source given by the following formula

$$\mathbf{f} = rck(t)(0, 0, 1)^T \delta(x) \delta(y) \delta(z - z_s),$$

where  $rck(t)$  is the Ricker wavelet, defined as

$$rck(t) = \left(1 - \frac{1}{2} \omega_p^2 t^2\right) e^{(-\frac{1}{4} \omega_p^2 t^2)},$$

Table 1. Layer properties to simulate propagation through stratified media

Property	Layer 1	Layer 2	Layer 3
Bulk density ( $Kg/m^3$ )	2200	2400	2200
Compressibility modulus ( $Pa$ )	$4.69 \times 10^9$	$2.69 \times 10^9$	$6.05 \times 10^9$
Shear modulus ( $Pa$ )	$3.46 \times 10^9$	$7.78 \times 10^9$	$1.46 \times 10^9$
Conductivity ( $S/m$ )	0.2	0.1	0.3

where  $\omega_p = 80 \text{ rad/s}$  is the dominant frequency.

We simulate the  $P$ - and  $S$ -wave propagation when the stratified medium consists of three layers: layer 1 has a depth of  $1000 \text{ m}$ , and the upper boundary is a free surface in contact with air; layer 2 has a depth of  $500 \text{ m}$ , the upper interface is in contact with layer 1; and the lower interface is in contact with layer 3, where layer 3 has an infinite depth. The characteristics of the three layers are in Table 1. Thus, in Figures 1 and 2 we observe the seismic trace with several events that record the  $P$ - or  $S$ -wave arrival times. We see reflected waves on the first or second interfaces, as well as their multiples.

We observe in Figure 1 the seismic trace of an elastic wave in the simulation where the source and the receiver are at the same position on the free surface. To interpret this seismic trace given by the matrix method, we compare the arrival times of several types of waves, see Table 2, with arrival times in the trace. Table 2 was built using the properties of the medium in layer 1 and layer 2 of Table 1, and shows arrival times of  $P$ - and  $S$ -wave, and  $PS$ -conversion, reflected on the first or second interfaces. The arrival times in Table 2 are calculated using the following expressions for the velocities of  $P$ - and  $S$ -waves

$$V_P = \sqrt{\frac{\lambda + 2G}{\rho}} \quad \text{and} \quad V_S = \sqrt{\frac{G}{\rho}}.$$

Therefore, using Table 2 and the output given by the matrix method in Figure 1, we outline some observations about the seismic propagation:

The receiver and the source are placed at the same position on the surface, so Event 1 at time zero records the direct wave. Note that the blue phase in Event 1 is similar to Ricker pulse (no dispersion effect) and the red phase is not significant (no attenuation effect) since the wave did not propagate yet. Event 2 occurs at the required time (row 1 of Table 2) for the  $P$ -wave to propagate back and forth between the surface and the first interface, so Event 2 records the reflection of the  $P$ -wave on the first interface. The amplitude of Event 2 is much smaller than the amplitude of Event 1, due to both the loss of energy while propagating and mainly due to the wave transmitted to the second layer. Event 3 occurs at the required time for the  $P$ -wave to be re-

flected on the second interface, as we see in row 3 of Table 2. The Event 3 also occurs in the necessary time (row 2 of Table 2) for the  $PS$ -conversion when reflected on the first interface. The simultaneous arrival of these two waves may explain why the amplitude of Event 3 is greater than the amplitude of Event 2. The arrival time (row 4) of Event 4 is required for the  $S$ -wave be reflected on the first interface. Event 5 has twice the arrival time (row 5) and a smaller amplitude than Event 2, that is, Event 5 is a multiple of the  $P$ -wave reflected on the first interface. Event 5 has a much smaller amplitude than Event 2 because of the difference in travel distance and because Event 2 faces only one loss of energy at the interface (one reflection) while event 5 faces two losses of energy at the interface (two reflections, considering the total reflection below the free surface). Event 6 records the reflected  $S$ -wave on the second interface as we can check on row 7 in Table 2. Event 6 is also the arrival time (row 6) of the  $PS$ -conversion when the conversion occurs at the second reflection on the first interface. The simultaneous arrival of these two waves may explain why the amplitude of Event 6 is greater than the amplitude of Event 4. Event 7 has twice the arrival time (row 8) of Event 3; it is a multiple of the  $P$ -wave reflected on the second interface. Event 8 is three times the arrival time (row 9) of Event 2; it is the second multiple of the  $P$ -wave reflected on the first interface. The seismic trace shows no precision after Event 8. For example, the row 10 of Table 2 shows the arrival time of the multiple of  $S$ -wave reflected on the first interface at  $3.1896 \text{ s}$ , but the most close events in Figure 1 occur before that time. They are Event 9 at  $2.85 \text{ s}$  and Event 10 at  $2.99 \text{ s}$ , approximately. Another example is the arrival of the third multiple of  $P$ -wave reflected on the first interface (row 11), whose closest event is 11 at  $3.34 \text{ s}$ .

In the second simulation of mechanical waves, the source-receiver distance is  $750 \text{ m}$ , while we place the source on the free surface and the receiver vertically below the source. In Figure 2, we observe the arrival of the direct wave (Event 1) for the same model as Figure 1, and the only difference is the source-receiver distance. Comparing Event 1, see Figures 1 and 2, the amplitude of the direct wave decreases due to the loss of energy to the medium while the wave propagates between source and receiver. We also observe dispersion effect (blue phase) and attenuation effect (red phase).

Table 2. Arrival times of several elastic waves

Rows	Waves	Arrival times (s)
1	<i>P</i> -wave reflected at 1 <sup>st</sup> interface	0.8706
2	<i>PS</i> -conversion at 1 <sup>st</sup> interface	1.2327
3	<i>P</i> -wave reflected at 2 <sup>nd</sup> interface	1.2333
4	<i>S</i> -wave reflected at 1 <sup>st</sup> interface	1.5948
5	1 <sup>st</sup> multiple of <i>P</i> -wave reflected at 1 <sup>st</sup> interface	1.7412
6	<i>PS</i> -conversion when reflected twice at 1 <sup>st</sup> interface	2.1033
7	<i>S</i> -wave reflected at 2 <sup>nd</sup> interface	2.1502
8	multiple of <i>P</i> -wave reflected at 2 <sup>nd</sup> interface	2.4665
9	2 <sup>nd</sup> multiple of <i>P</i> -wave reflected at 1 <sup>st</sup> interface	2.6118
10	multiple of <i>S</i> -wave reflected at 1 <sup>st</sup> interface	3.1896
11	3 <sup>rd</sup> multiple of <i>P</i> -wave reflected at 1 <sup>st</sup> interface	3.4825
12	multiple of <i>S</i> -wave reflected at 2 <sup>nd</sup> interface	4.3004

Since the receiver is close to the first interface, the first reflection in Figure 2 occurs earlier than in Figure 1, at 5.1 s, and it is very close to the direct wave.

**Note 5** Our simulations using the Ursin matrix method are implemented symmetrically around the origin. This approach is interesting for better visualization of the direct wave when the source and receiver are placed in the same position and when we are working with non-causal functions to simulate a seismic source; see, for instance, Madariaga (2015). Note that in the electromagnetic case, the formulas obtained in the Appendix are asymmetric with respect to  $\omega \in [-\omega_N, \omega_N]$ , where  $\omega_N$  is the Nyquist frequency. Although some minor adaptations of the algorithm reflected the asymmetry are required, we have some implementation advantages because the Ricker pulse and its Fourier transform are symmetric. We also remark that there is no computational cost much higher than the conventional approach since the intervals  $[0, 2\omega_N]$  and  $[-\omega_N, \omega_N]$  are the same size. In the elastic case, there is no such need due to the symmetry of the corresponding formulas with respect  $\omega \in [-\omega_N, \omega_N]$ . In general, this is a consequence of the fact that the Lamé system does not change when  $\omega$  is replaced by  $-\omega$ , while Maxwell's system (with  $\sigma \neq 0$ ) changes.

**Electromagnetic waves simulation**

Consider a particular case of the electromagnetic source given by

$$\mathbf{j} = \mathbf{j}^0 \delta(x) \delta(y) \delta(z - z_s), \quad z_s \rightarrow 0^+,$$

where  $\mathbf{j}^0 = (j_1^0, j_2^0, j_3^0)^T$ , and  $j_i^0, i = 1, 2, 3$ , are strongly concentrated functions in the frequency domain given by

$$j_i^0(\omega) = \frac{2\omega^2}{\sqrt{\pi}\omega_p^3} e^{-\frac{\omega^2}{\omega_p^2}}.$$

The simulation is done assuming  $\epsilon_0 = 8.854 \times 10^{-12} \text{ F/m}$  and  $\mu_0 = 4\pi \times 10^{-7} \text{ [Tm/A]}$ .

The results presented in Figure 3 were obtained for the case of a stratified medium consisting of three layers, where the thickness of the first layer is 2000 m, the second is 1000 m, and the thickness of the third layer is infinity; the source and receiver are at the same position on the free surface  $z = 0$ .

Let's highlight some characteristics of the electromagnetic trace in Figure 3. Event 1 records the direct wave and occurs at the beginning of time since the receiver and source are located at the same position on the surface. Note that the phase is similar to Ricker's pulse. Event 2, at time 0.025 s, records the arrival of the wave reflected on the first interface, at 2000 m deep. This depth and this arrival time show the wave's speed is on the order of  $10^4 \text{ m/s}$ , as expected in this kind of media. Event 3 occurs at the time required for the wave to be reflected on the second interface at 3000 m deep. Event 4 occurs twice the time of Event 2. It is the multiple of the reflected wave on the first interface. The amplitude of Event 2 is not much smaller than the amplitude of Event 1, and the amplitude of Event 4 is not much smaller than the amplitude of Event 2, suggesting the waves undergo total reflection in the free surface. The amplitude decreases almost exclusively due to both the loss of energy in the propagation medium and the reflection on the first interface (energy trans-

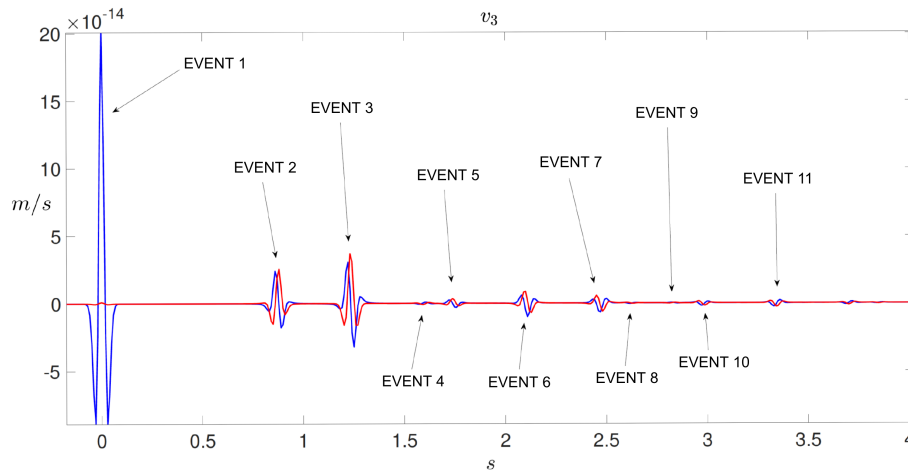


Figure 1. Mechanical propagation in 3D half-space, where the thickness of the first layer is  $1000\text{ m}$ ; the second,  $500\text{ m}$ , and the source and receiver are at the same position on the free surface

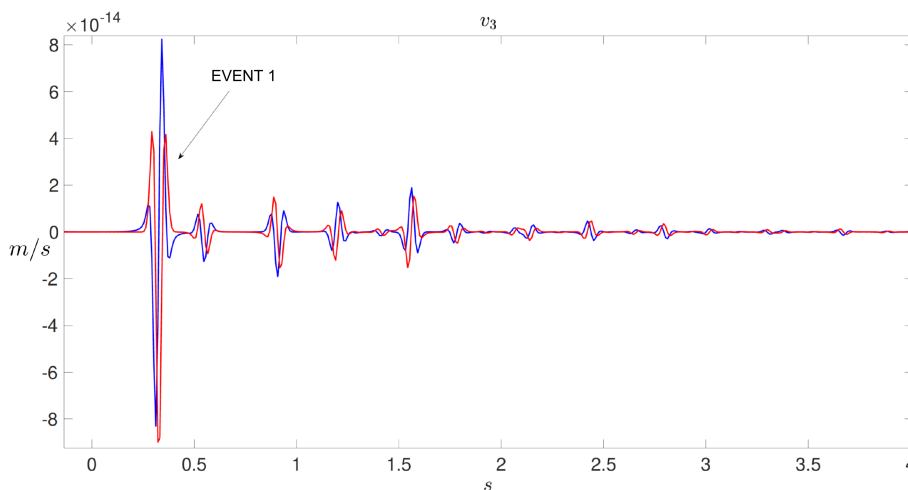


Figure 2. Mechanical propagation in 3D half-space, where the thickness of the first layer is  $1000\text{ m}$ ; the second,  $500\text{ m}$ , the source is on the free surface, and the receiver is at a depth of  $750\text{ m}$  vertically below the source

mitted to second layer). Despite the propagation over a greater distance, the amplitude of Event 4 is greater than the amplitude of Event 3, because in Event 4 the wave undergoes two moments of energy loss (two reflections), while in Event 3 the wave undergoes three moments of energy loss (two transmissions and one reflection). The phases show prolonged oscillations, not observed in mechanical cases and it is possibly due to reverberation phenomena. The trace also shows small variations between events that do not happen in mechanical simulations. They may have been generated due to a lack of precision or numerical instabilities.

Figure 4 shows the results of the second experiment using the same parameters as in the previous simulation shown in Figure 3, with the only difference that this time the thickness of the second layer is  $3000\text{ m}$ . Following Figure 4, we list some observations: Since source and receiver are in the same position, Event 1 occurs at time zero. Event 2 records the arrival of the wave reflected on the first interface. Since we have not changed the first layer characteristics, Event 2 in

Figure 4 shows the same amplitude and arrival time as Event 2 in Figure 3. Event 3 is twice of the arrival time of Event 2, therefore it is the multiple of the wave reflected on the first interface. Again, as we did not change the first layer's characteristics, Event 3 in Figure 4 shows approximately the same amplitude and arrival time as Event 4 in Figure 3. Event 4 in Figure 4 occurs at the time required for the wave to reflect on the second interface, which is  $5000\text{ m}$  deep. Observe that Event 4 corresponds to Event 3 in Figure 3, but shows a slightly smaller amplitude, slightly longer oscillations and greater travel time. Event 5 has three times the arrival time of Event 2. It is the arrival of the second multiple of the wave reflected in the first interface. Event 4 occurs sooner than Event 5 but has a smaller amplitude. The wave that generated Event 4 propagates through two layers, while the wave from Event 5 propagates only in the first layer. Possibly, the transmission phenomena cause more significant energy loss than the reflection phenomena.

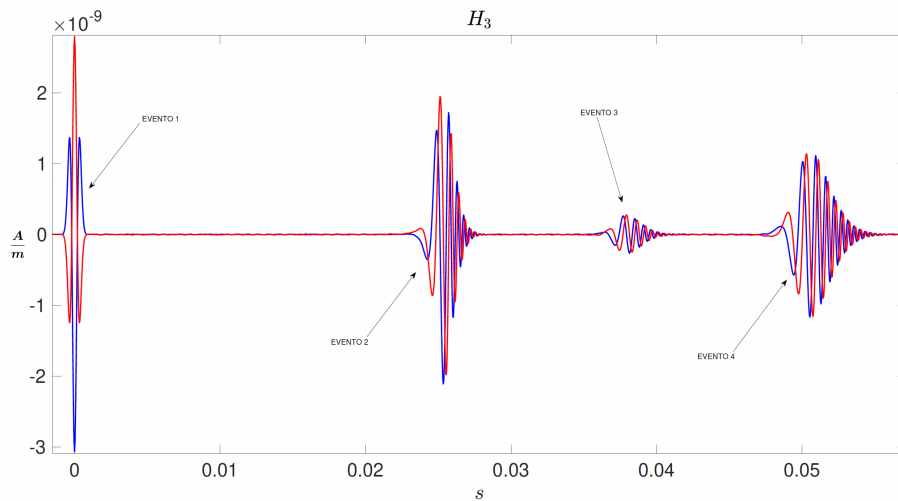


Figure 3. Electromagnetic propagation in 3D half-space, where the thickness of the first layer is 2000  $m$ , the second is 1000  $m$ , and the source and receiver are at the same position on the free surface

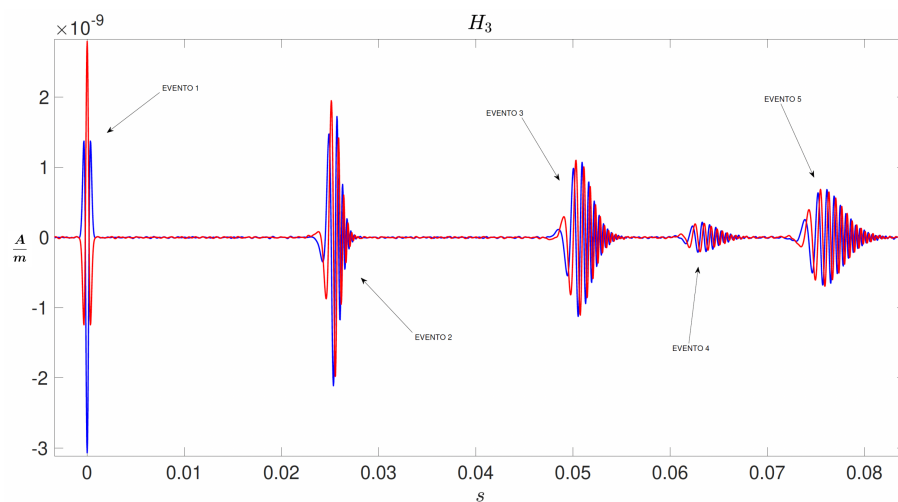


Figure 4. Electromagnetic propagation in 3D half-space, where the thickness of the first layer is 2000  $m$ , the second is 3000  $m$ , and the source and receiver are at the same position on the free surface

## CONCLUSION

In this article, we presented and numerically performed the Ursin matricial method in the case of the elastic and electromagnetic waves propagated in the 3D stratified media. We found out that the proposed algorithm effectively simulates the  $P$ - and  $S$ -waves propagation and the  $PS$ -conversion, and it is also useful for modeling the electromagnetic waves.

In the case of electromagnetic waves, to describe the process of propagation of waves in the air, we used the complete (hyperbolic) version of Maxwell's equations; and in the Earth's subsurface, the diffusion (parabolic) version. Applying the boundary conditions (14) and (15), we were able to reduce the study area of the corresponding problem to the 3D half-space simulating the Earth's interior, thus reducing the numerical algorithm computational cost keeping the impact of the air half-space.

## ACKNOWLEDGMENTS

The authors would like to thank anonymous referees for the careful reading of this paper and stimulating comments and suggestions. The first author was supported by the Coordination of Researchers' Improvement - CAPES. This work was prepared with support of the Laboratory of Engineering and Exploration of Petroleum - LENEP of the State University of Norte Fluminense Darcy Ribeiro - UENF, Macaé, RJ, Brazil.

## APPENDIX A.

In this Appendix, we represent the explicit formulas for calculation of the eigenvalues and eigenvectors mentioned in Section Ursin Method for the considered elastic and electromagnetic problems.

**Elastic problem**

**System 1.** There are two waves modes: fast compressional wave or *P*-wave ( $j = 1$ ) and vertical shear wave or *SV*-wave ( $j = 2$ ). In this case, the two distinct nonzero eigenvalues  $q_j^2$  of matrices  $\mathbf{M}_1\mathbf{M}_2$  and  $\mathbf{M}_2\mathbf{M}_1$  are:

$$q_j^2 = \frac{1}{2} \left[ \frac{\rho}{\lambda + 2G} + \frac{\rho}{G} - 2\gamma^2 \pm \sqrt{\left( \frac{\rho}{\lambda + 2G} - \frac{\rho}{G} \right)^2 + \left( \frac{\beta_1\rho}{\lambda + 2G} + \frac{\beta_2\rho}{G} \right) \gamma^2} \right],$$

where  $j = 1, 2$ , the signals (+) and (-) are for  $j = 1$  and  $j = 2$ , respectively; and

$$\beta_1 = 16 + \frac{8\lambda}{\lambda + 2G} \quad \text{and} \quad \beta_2 = 4 + \frac{4\lambda^2}{(\lambda + 2G)^2}.$$

The corresponding eigenvectors are

$$\mathbf{a}_1^{(1)} = \sqrt{\frac{q_1}{\rho + 2\gamma a_1 + \frac{a_1^2}{G}}} (1, a_1)^T,$$

$$\mathbf{a}_2^{(1)} = \sqrt{\frac{q_2}{a_2^2\rho + 2\gamma a_2 + \frac{1}{G}}} (a_2, 1)^T,$$

where

$$a_1 = \frac{q_1^2 - \frac{1}{\lambda + 2G}}{\frac{\gamma\lambda}{\lambda + 2G}} \quad \text{and} \quad a_2 = \frac{\frac{\gamma\lambda}{\lambda + G}}{q_2^2 - \frac{1}{\lambda + 2G}},$$

and

$$\mathbf{b}_1^{(1)} = \frac{1}{q_1} \mathbf{M}_2^{(1)} \mathbf{a}_1^{(1)}, \quad \mathbf{b}_2^{(1)} = \frac{1}{q_2} \mathbf{M}_2^{(1)} \mathbf{a}_2^{(1)}.$$

**System 2.** There is only the horizontal shear wave (*SH*-wave). The corresponding eigenvalue  $q^2$  is calculated by

$$q^2 = \frac{\rho}{G} - \gamma^2,$$

and the eigenvectors are

$$\mathbf{a}^{(2)} = \sqrt{\frac{q}{\rho - G\gamma^2}}, \quad \mathbf{b}^{(2)} = \sqrt{\frac{\rho - G\gamma^2}{q}}.$$

**Electromagnetic problem**

**System 1.** In this case, the eigenvalue  $q^2$  is given by

$$q^2 = -\frac{\mu_0\bar{\sigma}}{i\omega} - \gamma^2,$$

and the eigenvectors are

$$\mathbf{a}^{(1)} = \sqrt{\frac{q}{-\mu_0 - \frac{i\omega\gamma^2}{\bar{\sigma}}}}, \quad \mathbf{b}^{(1)} = \frac{1}{q} \left( -\mu_0 - \frac{i\omega\gamma^2}{\bar{\sigma}} \right) \mathbf{a}^{(1)}.$$

**System 2.** The corresponding eigenvalue  $q^2$  is calculated by

$$q^2 = -\frac{\mu_0\bar{\sigma}}{i\omega} - \gamma^2,$$

and the eigenvectors are

$$\mathbf{a}^{(2)} = \sqrt{\frac{q}{\frac{\bar{\sigma}}{i\omega} + \frac{\gamma^2}{\mu_0}}}, \quad \mathbf{b}^{(2)} = \frac{1}{q} \left( \frac{\bar{\sigma}}{i\omega} + \frac{\gamma^2}{\mu_0} \right) \mathbf{a}^{(2)}.$$

**REFERENCES**

Azeredo, A.; Priimenko, V. An algorithm for wave propagation analysis in stratified poroelastic media. *Eurasian Journal of Mathematical and Computer Applications* **2015**, *3*, 55–69.

Bracewell, R. *The Fourier transform and its applications*; McGraw-Hill, 1978.

Brekhovskih, L. *Waves in layered media*; New York: Academic Press, 1960.

Griffiths, D. *Introduction to electrodynamics*; N.J.: Prentice-Hall, 1999.

Haarsten, M.; Pride, S. Electro seismic waves from point sources in layered media. *J. Geophys. Res.* **1997**, *102*, 24745–24796.

Haskell, N. The dispersion of surface waves on multilayered media. *Bull. Seismol. Soc. Am.* **1953**, *43*, 17–43.

Kunetz, G.; D’Erceville. Sur certaines propriétés d’une onde acoustique plane de compression dans un milieu stratifié. *Ann. de Geophys.* **1962**, *18*, 351–359.

Mackay, T.; Lakhtakia, A. The transfer-matrix method in electromagnetics and optics. *Synthesis lectures on electromagnetics* **2020**, *1*, 1–126.

Madariaga, R. Seismic source theory. *Treatise on geophysics* **2015**, *4*, 51–71.

Miranda, M.; Priimenko, V. An algorithm for calculating reflected/transmitted poroelastic waves across all frequencies. *Eurasian Journal of Mathematical and Computer Applications* **2017**, *5*, 4–15.

Molotkov, L. *Matrix method in the theory of wave propagation in layered elastic and fluid media*; Leningrad: Nauka, 1984.

Oliveira, I.; Azeredo, M.; Miranda, M.; Priimenko, V. Poroelastic modeling in stratified media across all frequencies. *Brazilian Journal of Geophysics* **2018**, *36*, 581–596.

Pride, S.; Haarsten, M. Electro seismic wave properties. *J. Acoust. Soc. Am.* **1996**, *100*, 1301–1315.

Sokolnikoff, I. *Mathematical theory of elasticity, 2nd ed.*; Bombay - New Delhi: McGraw-Hill, 1946.

Thomson, W. Transmission of elastic waves through a stratified solid medium. *J. Appl. Phys.* **1950**, *21*, 89–93.

Tygel, M.; Hubral, P. *Transient waves in layered media, 1ed.*; Elsevier Science, 1987.

Ursin, B.; Stovas, A. Reflection and transmission responses of layered isotropic viscoelastic media. *Geophysics* **2002**, *67*, 307–323.

Ursin, B. Review of elastic and electromagnetic wave propagation in horizontally layered media. *Geophysics* **1983**, *48*, 1063–1081.

White, B.; Zhou, M. Electro seismic prospecting in layered media. *SIAM J. APPL. MATH.* **2006**, *67*, 307–323.

**D.P.:** Computational implementation of the method, elaboration of the workflow, numerical modeling, generation and analysis of the results. **V.P and M.A.:** Development of mathematical basis, construction of the workflow and analysis of the results.

Received on February 17, 2021/ Accepted em August 25, 2021.



-Creative Commons attribution-type BY